Non-volatile Electrically Reconfigurable Optical MZI Integrated with Sb_2Se_3 Sub-cell Arrays for High Endurance Switching

Xing Yang(1), Liangjun Lu(1), Yu Li(1), Jianping Chen(1), Linjie Zhou(1)

(1) State Key Laboratory of Advanced Optical Communication Systems and Networks, Shanghai Key Lab of Navigation and Location Services, Shanghai Institute for Advanced Communication and Data Science, Department of Electronic Engineering, Shanghai Jiao Tong University, Shanghai 200240, China, luliangjun@sjtu.edu.cn, ljzhou@sjtu.edu.cn

Abstract *We demonstrated an electrical-driven non-volatile MZI based on low-loss Sb_2Se_3 sub-cell arrays. By constraining the material reflow in the sub-cells, optical transmission contrast of > 5 dB was achieved with > 1000 phase-change cycles.*

Introduction

As the semiconductor manufacturing process advances toward the 3-nm node, electronic devices based on Field Programmable Gate Arrays (FPGAs) or Von Neumann architecture show signs of lagging in high-speed and low-power signal processing due to the limitation of Moore's Law. Recently, the concept of programmable optical signal processor (POSP) has been proposed and several prototype chips have been demonstrated, showing the potential for multi-functional optical signal processing [1, 2]. Similar to electronic FPGAs, the POSP system is achieved by constructing an integrated optical hardware network with many programmable interconnection nodes, mainly relied on basic optical tunable couplers such as Mach–Zehnder interferometers (MZIs) and microrings [3, 4]. However, the weak refractive index tuning schemes based on the thermo-optic (TO) or electro-optic (EO) effects limit the further reduction of the device size. Moreover, continuous power consumption is required to maintain the states of the optical tunable couplers due to the volatile property.

Phase change materials (PCMs) integrated silicon photonics have recently attracted great interests due to the large refractive index difference between amorphous and crystalline states, which allow a smaller phase shifter size for π-shift [5-7]. In addition, the self-holding property of PCMs means that once the state is changed, no static power is needed to maintain the states of PCMs. However, non-volatile optical devices with PCMs such as $Ge_2Sb_2Te_5$ (GST) and $Ge_2Sb_2Se_4Te_1$ (GSST) suffer from large absorption loss due to the large imaginary refractive index of GST and GSST in the crystalline state [8-10]. Several low-loss PCMs have been reported, including Sb_2S_3 (SbS) and Sb_2Se_3 (SbSe), which can provide a relatively large real part difference (0.6 for SbS and 0.77 for SbSe) of the refractive index between the crystalline and amorphous states, while having a much smaller imaginary part than GST and GSST at the wavelength of 1550 nm [11]. Phase shifters based on SbS-Si and SbSe-Si hybrid integrated waveguides have been reported, and effectively reduce the length for π-shift by almost two orders compared with the EO and TO shifters [12, 13]. However, the degradation of the device performance caused by the material deformation during the phase change process poses a serious challenge to the application of POSP [12, 14].

In this paper, we demonstrate an electrically driven non-volatile optical MZI consisting of the SbSe-Si phase shifter on a p-i-n-diode-based heater. To restrict the reflow of SbSe during the phase change process, the SbSe is patterned into small cell arrays. Besides, two layers of Al_2O_3 are deposited separately to encapsulate each SbSe sub-cell and provide electrical isolation with the p-i-n heater. The device shows good endurance of more than 1000 cycles during the phase change process. Transmission electron microscopy (TEM) analysis of the small SbSe cell arrays after many phase change cycles indicates that this is an effective method for reducing SbSe reflow.

Device structure

Figure 1(a) shows the schematic structure of the SbSe-Si hybrid integrated phase shifter fabricated on the silicon-on-insulator (SOI) platform. To integrate with the p-i-n heater, the Si strip waveguide is transitioned to a ridge waveguide with a 150-nm-thick slab by a linear taper. The width of the ridge is set to 1.2 μm to improve the manufacturing tolerance. The slabs on both sides of the ridge waveguide are highly doped with boron and phosphorus to form the p-i-n diode. As shown the inset of Figure 1(a), the P^{++} and N^{++} regions are separated from the waveguide sidewalls by 0.7 μm to avoid doping absorption loss. A 20/150 nm thick Cr/Au layer is located above the highly doped regions to form an ohmic contact. The SbSe layer is sandwiched by two layers of Al_2O_3 with the bottom layer thickness of 10 nm and the top layer thickness of 40 nm to electrically isolate with the p-i-n heater and prevent the SbSe from oxidation. The thickness of SbSe is 30 nm. The period of the SbSe sub-cell arrays is 600 nm and the gap between SbSe cells is 100 nm. The length of the SbSe-Si phase shifter is 18 μm. Figure 1(b) shows the Scanning Electron Microscopy (SEM) image of the fabricated MZI integrated with Si-SbSe phase shifter. It consists of two multimode interferometers (MMI) connected by two waveguide arms. Grating couplers are used to couple the transverse electric (TE) polarized light into and out of the waveguide. The inset shows a zoomed view of the active region with SbSe arrays.

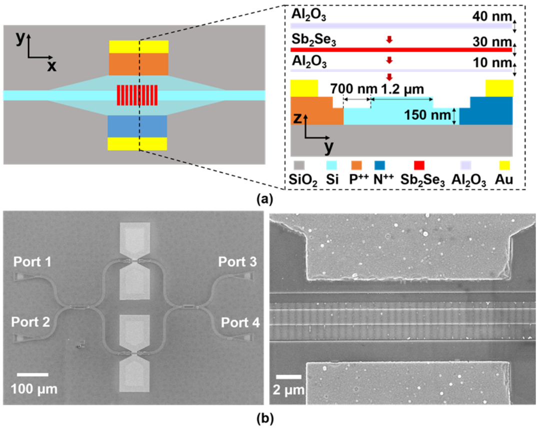

Fig. 1: (a) Schematic structure of the SbSe-Si phase shifter driven by a p-i-n heater. The inset shows the cross-sectional view of the phase shifter. (b) SEM image of the fabricated MZI with the SbSe-Si phase shifters integrated on arms. The inset shows the enlarged image of the phase shifter with SbSe arrays.

Experimental results

We investigated the amorphization and crystallization processes by adjusting the electrical pulses applied to the p-i-n heater. The SbSe was initially in the crystalline state after atomic layer deposition (ALD) of Al_2O_3 at the temperature of 250 ℃ during the device fabrication process. Due to the initial phase error, the device was not exactly at the cross-state. As shown in Figure 2(a), by applying a series of amorphization pulses with the pulse width fixed at 100 ns and the amplitude increased from 7 V to 9.5 V with a step of 0.5 V, the optical transmission from Port 1 to Port 3 was gradually reduced when the MZI was tuned close to the cross-state. The transmission level was maintained after each pulse, indicating the non-volatile property of our device. The optical power was nearly unchanged when the amplitude was lower than 8 V since the temperature of SbSe was lower than its amorphization temperature. For recrystallization, series of electrical pulses with an increased amplitude from 3 V to 3.8 V and a step of 0.2 V were applied to the phase shifter. The pulse width was fixed at 20 μs and the pulse interval was 1 s to allow a long cooling time. As shown in Figure 2(b), the optical power from Port 3 gradually increases with the applied electrical pulses, indicating that the phase difference between the two arms of the MZI can be reversibly tuned by changing the state of SbSe. Figures 2(c) and (d) show the second phase change cycle. The slight difference in optical transmission from the first cycle is due to the morphological change of the material in its phase transition process.

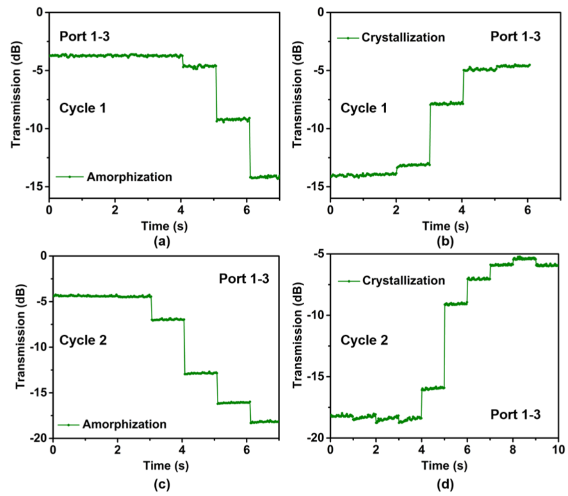

Fig. 2: (a-d) Transmission variation of the Path 1-3 of the device for two cycles of (a, c) amorphization and (b, d) crystallization process.

To investigate the endurance of the device, we applied 1250 cycles of electric pulses (9.5 V, 120 ns for amorphization and 3.7 V, 20 μs for crystallization) with a period of 1 s and recorded the optical transmission change. The switching energy was 108 nJ and 1.4 μJ for single amorphization and crystallization pulses, respectively. As shown in Figure 3(a), the transmission contrast is greater than 5 dB throughout the long test period. In comparison, we also tested a MZI with a whole piece of SbSe on the p-i-n heater. To be noted, the device also has two Al_2O_3 layers for protection. Figure 3(d) shows the optical transmission change of the MZI with a whole SbSe strip after 1000 cycles. Transmission contrast is reduced from over 15 dB to about 3 dB, which indicates the gradual deformation of SbSe in the phase-change cycles.

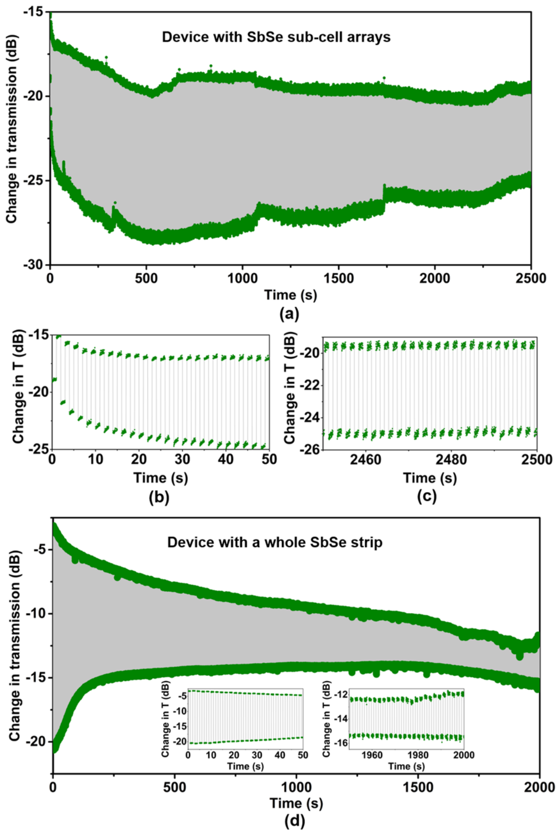

Fig. 3: (a) Reversible cycling test of 1250 switching periods for the device with SbSe sub-cell arrays. The pulse interval is 1 s. (b, c) Optical transmission change for the (b) first and (c) last 25 cycles. (d) Reversible cycling test of 1000 switching periods for the device with a whole SbSe strip.

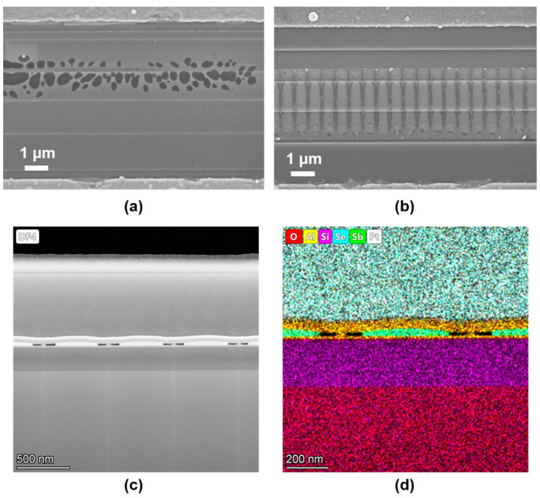

Fig. 4: SEM images of the Si-SbSe phase shifter for (a) strip after 1000 cycles and (b) array after 1250 cycles. (c, d) TEM images and corresponding EDS mappings of the phase shifter along the waveguide propagation direction with the SbSe arrays.

Figures 4(a) and (b) show the SEM images of the SbSe-Si phase shifter with the whole SbSe strip after 1000 cycles and the SbSe sub-cell arrays after 1250 cycles, respectively. There are many randomly distributed voids in the SbSe strip. For the SbSe sub-cell arrays, the voids are mainly formed at the waveguide edges. Figures 4(c) and (d) show the TEM image and corresponding energy dispersive spectroscopy (EDS) mappings of the SbSe-Si phase shifter with SbSe sub-cell arrays along the waveguide propagation direction. The distribution of voids implies the division of SbSe into small sub-cells can effectively reduce the material reflow along the longitudinal direction. The reflow can be further inhibited by designing narrower SbSe sub-cells within the waveguide width.

Conclusion

In summary, we have demonstrated a non-volatile electrically reconfigurable MZI integrated with a SbSe-Si phase shifter in each waveguide arm. The SbSe phase change is electrically driven by a silicon p-i-n heater. The state of the MZI can be reversibly switched by changing the state of the SbSe. Due to the material isolation of SbSe sub-cell arrays and a better protection of the dual Al_2O_3 layers, the performance of the device has no significant deterioration after more than 1000 phase-change cycles. The TEM and EDS results also indicate the reflow of the material can be effectively inhibited by using SbSe small patch arrays, which is significant to improve the performance stability of the PCM based optical devices for POSP application.

Acknowledgements

This work was supported in part by the National Key R&D Program of China (2021YFB2801300), and the National Natural Science Foundation of China (62090052, 62135010, 62075128). The authors thank the Center for Advanced Electronic Materials and Devices (AEMD) of Shanghai Jiao Tong University (SJTU) for support in device fabrication.

References

[1] D. Pérez, I. Gasulla, P. Das Mahapatra, and J. Capmany, "Principles, fundamentals, and applications of programmable integrated photonics," Advances in Optics and Photonics, vol. 12, no. 3, p. 709, 2020, doi: 10.1364/aop.387155.

[2] J. Feldmann et al., "Parallel convolutional processing using an integrated photonic tensor core," Nature, vol. 589, no. 7840, pp. 52-58, Jan 2021, doi: 10.1038/s41586-020-03070-1.

[3] D. Marpaung, J. Yao, and J. Capmany, "Integrated microwave photonics," Nature Photonics, vol. 13, no. 2, pp. 80-90, 2019, doi: 10.1038/s41566-018-0310-5.

[4] B. J. Shastri et al., "Photonics for artificial intelligence and neuromorphic computing," Nature Photonics, vol. 15, no. 2, pp. 102-114, 2021, doi: 10.1038/s41566-020-00754-y.

[5] Z. Cheng, C. Rios, N. Youngblood, C. D. Wright, W. H. P. Pernice, and H. Bhaskaran, "Device-Level Photonic Memories and Logic Applications Using Phase-Change Materials," Adv Mater, vol. 30, no. 32, p. e1802435, Aug 2018, doi: 10.1002/adma.201802435.

[6] C. Wu, H. Yu, H. Li, X. Zhang, I. Takeuchi, and M. Li, "Low-Loss Integrated Photonic Switch Using Subwavelength Patterned Phase Change Material," ACS Photonics, vol. 6, no. 1, pp. 87-92, 2018, doi: 10.1021/acsphotonics.8b01516.

[7] H. Zhang et al., "Miniature Multilevel Optical Memristive Switch Using Phase Change Material," ACS Photonics, vol. 6, no. 9, pp. 2205-2212, 2019, doi: 10.1021/acsphotonics.9b00819.

[8] Y. Zhang et al., "Broadband transparent optical phase change materials for high-performance nonvolatile photonics," Nat Commun, vol. 10, no. 1, p. 4279, Sep 30 2019, doi: 10.1038/s41467-019-12196-4.

[9] J. Zheng et al., "Nonvolatile Electrically Reconfigurable Integrated Photonic Switch Enabled by a Silicon PIN Diode Heater," Adv Mater, vol. 32, p. e2001218, Jun 26 2020, doi: 10.1002/adma.202001218.

[10] R. Chen, Z. Fang, J. E. Fröch, P. Xu, J. Zheng, and A. Majumdar, "Broadband Nonvolatile Electrically Controlled Programmable Units in Silicon Photonics," ACS Photonics, vol. 9, no. 6, pp. 2142-2150, 2022, doi: 10.1021/acsphotonics.2c00452.

[11] M. Delaney, I. Zeimpekis, D. Lawson, D. W. Hewak, and O. L. Muskens, "A New Family of Ultralow Loss Reversible Phase‐Change Materials for Photonic Integrated Circuits: Sb2S3 and Sb2Se3," Advanced Functional Materials, p. 2002447, 2020, doi: 10.1002/adfm.202002447.

[12] M. Delaney et al., "Nonvolatile programmable silicon photonics using an ultralow-loss Sb2Se3 phase change material," (in English), Science Advances, vol. 7, no. 25, Jun 2021, doi: ARTN eabg3500 10.1126/sciadv.abg3500.

[13] C. Ríos et al., "Ultra-compact nonvolatile phase shifter based on electrically reprogrammable transparent phase change materials," PhotoniX, vol. 3, no. 1, 2022, doi: 10.1186/s43074-022-00070-4.

[14] Z. Fang et al., "Ultra-low-energy programmable non-volatile silicon photonics based on phase-change materials with graphene heaters," Nat Nanotechnol, Jul 4 2022, doi: 10.1038/s41565-022-01153-w.